Auger decay in dispersing and absorbing environments

Janine Franz,[1] Robert Bennett,[1,2] and Stefan Yoshi Buhmann[1,3]

[1] *Physikalisches Institut, Albert-Ludwigs-Universität Freiburg, Hermann-Herder-Str. 3, 79104 Freiburg, Germany*
[2] *School of Physics & Astronomy, University of Glasgow, Glasgow, G12 8QQ, United Kingdom*
[3] *Institut für Physik, Universität Kassel, Heinrich-Plett-Straße 40, D-34132 Kassel, Germany*

(Dated: June 29, 2021)

We develop a quantum-optical description of Auger decay, which is an ultra-fast, high-energy autoionisation process, on the basis of macroscopic quantum electrodynamics. One consequence of the new perspective is a simple analytical formula for the free-space Auger rate which we compare with available rates of the F-like isoelectronic sequence. More importantly, the formalism enables us to study the Auger decay in different dispersing and absorbing environments. We show that in contrast to common assumptions the Auger rate can be influenced by environment, presenting two simple examples, namely a dielectric surface and a surrounding bulk medium.

I. INTRODUCTION.

Quantum optics and quantum chemistry provide complementary descriptions of resonant energy transfer. Quantum optics traditionally deals with propagating photon-like excitations, while quantum chemistry deals with short-range, electrostatic correlations between charge distributions. An energy transfer process that has traditionally been studied by quantum optical methods is the Förster resonant energy transfer (FRET) [1], where an initially excited donor relaxes and the released energy is then absorbed by an acceptor, exciting it. This easy-to-access process has been an invaluable tool across the sciences for decades [2, 3].

When using an highly excited donor, the transferred energy can be sufficient to ionise the acceptor. This much faster process is known as interatomic Coulombic decay (ICD) [4], and has received increasing attention due to its production of a low-energy electron [5, 6]. Retardation effects at farther distances as well as a Purcell-type influence of dispersing and absorbing environments [7, 8] can be included using the formalism of macroscopic quantum electrodynamics (QED) [9] by its description through body-field polaritonic excitations [10].

At even higher energies, a new relaxation channel opens, the Auger decay [11, 12]. This is an autoionisation process, where one and the same atom serves as donor and acceptor. Auger decay finds application in Auger electron spectroscopy and is crucial for astrophysical modelling [13, 14]. In contrast to FRET, where quantum chemistry plays a subordinate role, ab initio quantum chemistry calculations have been the main tool for prediction of Auger decay rates. Quantum chemistry methods are suited for the descriptions of many–electron effects, but cannot take into account the influence of macroscopic environments. This is particularly important for the Auger decay due to its relevance to biological physics and radiation therapy [15, 16].

The sensitivity of Auger decay to the chemical environment of the self-ionising species is well established as the chemical shift in Auger spectra [17] and has also been observed near surfaces [18]. We show in this work that in analogy to the Purcell effect in spontaneous radiative decay or the recently studied fast and non-radiative ICD, the Auger rate may also be affected by the optical and electromagnetic properties of the environment, despite its non-radiative, high-energy, and ultrafast characteristics. With the current progress in x-ray quantum optics the Auger process can serve as an interesting high-energy analogue of the Purcell effect in radiative decay to be studied in an x-ray cavity. In the process we develop an analytical approximate formula for the Auger rate in free space, which is usually exclusively determined via quantum chemistry.

II. THEORY.

We use the framework of macroscopic QED to describe electromagnetic fields in Fourier space [10]. The vector potential is given by:

$$\hat{\boldsymbol{A}}(\boldsymbol{r}) = \int_0^\infty \mathrm{d}\omega \int \mathrm{d}V' \frac{\omega}{c^2}\sqrt{\frac{\hbar}{\pi\epsilon_0}\mathrm{Im}\varepsilon(\boldsymbol{r}',\omega)} \times {}^{\perp}\mathbf{G}(\boldsymbol{r},\boldsymbol{r}',\omega)\cdot\hat{\boldsymbol{f}}(\boldsymbol{r}',\omega) + \mathrm{h.c.} \tag{1}$$

where $\hat{\boldsymbol{f}}^{(\dagger)}(\boldsymbol{r},\omega)$ is the annihilation (creation) operator of a body–field polaritonic excitation at position $\boldsymbol{r}$ with an energy of $\hbar\omega$, $\mathbf{G}(\boldsymbol{r},\boldsymbol{r}',\omega)$ is the Green's tensor describing the propagation of these excitations from $\boldsymbol{r}'$ to $\boldsymbol{r}$ and ${}^{\perp}\mathbf{G}(\boldsymbol{r},\boldsymbol{r}')$ describes the transverse part of $\mathbf{G}$ with respect to the left argument $\boldsymbol{r}$.

Auger decay is an electron–electron scattering process, where two electrons start in state $|n,m\rangle$ and end up in state $|k,p\rangle$. Here $|k\rangle$ is the initial vacancy state and $|p\rangle$ is the continuum state of the emitted electron, see Fig. 1. The rate for this process is then given by: $\Gamma = \sum_f \frac{\partial}{\partial t}|\langle f|\hat{S}(t)|i\rangle|^2$, where $|i\rangle$, $|f\rangle$ are the initial and final states, respectively and $\hat{S}(t)$ is the scattering matrix, which we perturbatively expand in the interaction Hamiltonian $\hat{V}(t) = \int \mathrm{d}V \left[\hat{\rho}(\boldsymbol{r},t)\hat{\phi}(\boldsymbol{r},t) - \hat{\boldsymbol{j}}(\boldsymbol{r},t)\cdot\hat{\boldsymbol{A}}(\boldsymbol{r},t)\right]$. The lead-

ing contribution is of second-order [19]: $\hat{S}^{(2)}(t) = \frac{1}{\hbar^2}\int_{-\infty}^{t} \mathrm{d}t_a \int_{-\infty}^{t_a} \mathrm{d}t_b\, \hat{V}(t_a)\hat{V}(t_b)$. Making use of the low energy of the electrons, the Coulomb gauge as well as the continuity equation, we arrive at a general formula for the lowest contributing order:

$$\begin{aligned}\Gamma &= 2\pi \sum_f \delta(\omega_{kn} - \omega_{mp}) \left| V_{n\to k} - V_{m\to k} \right|^2 \\ &\equiv \Gamma_{\mathrm{dir}} + \Gamma_{\mathrm{exch}} + \Gamma_{\mathrm{intf}} \end{aligned} \tag{2}$$

with

$$\begin{aligned} V_{n\to k} &= \langle k, p | \hat{V} | n, m \rangle \\ &= \frac{\mu_0}{\hbar} \iint \mathrm{d}V_a \mathrm{d}V_b\; \boldsymbol{j}_{nk}(\boldsymbol{r}_a) \cdot \mathbf{G}_{ab}(\omega_{kn}) \cdot \boldsymbol{j}_{mp}(\boldsymbol{r}_b) \end{aligned} \tag{3}$$

and the shorthand notations $\mathbf{G}_{ab}(\omega_{kn}) = \mathbf{G}(\boldsymbol{r}_a, \boldsymbol{r}_b, \omega_{kn})$ and $\boldsymbol{j}_{nk}(\boldsymbol{r}_a) = \langle k | \hat{\boldsymbol{j}}(\boldsymbol{r}_a) | n \rangle$ for the time-independent transition current density. The transition energies are defined via $\omega_{kn} = \omega_n - \omega_k > 0$ and $\omega_{mp} = \omega_p - \omega_m > 0$. We may divide the rate into three parts: the direct and exchange rates Γ_{dir}, Γ_{exch}, given by the absolute square of the direct term $V_{n\to k}$ and the exchange term $V_{m\to k}$, respectively. The third contribution Γ_{intf} is given by the interference of the two, $\Gamma_{\mathrm{intf}} = V_{n\to k} V^*_{m\to k} + \mathrm{c.c.}$ In principle, expression (3) can be used as a new starting point for ab initio quantum chemistry calculation for any electron–electron scattering processes in any macroscopic environment described by $\mathbf{G}$. In free space one can use the respective Green's tensor [10] to show that our result is equivalent to the well-known Møller-formula [20].

III. DIPOLE APPROXIMATION.

The difficulty in the actual evaluation is that $\boldsymbol{j}_{nk}$ and $\boldsymbol{j}_{mp}$ are to be found from electronic structure calculations. To circumvent this, we introduce the dipole approximation: $\boldsymbol{j}_{nk}(\boldsymbol{r}_a) = \omega_{kn}\, \boldsymbol{d}_{nk}\, \delta(\boldsymbol{r}_a - \boldsymbol{r})$, where $\boldsymbol{d}_{nk} = \langle k | \hat{\boldsymbol{d}} | n \rangle$ is the transition dipole moment and $\boldsymbol{r}$ is the nuclear position. Relating the continuum-transition dipole $\boldsymbol{d}_{mp}$ to the photoionisation cross section σ_m of the state $|m\rangle$ [21], we obtain:

$$\begin{aligned}\Gamma_{\mathrm{dir}} + \Gamma_{\mathrm{exch}} =& \sum_{n,m} 18\pi c_{nkm} \gamma_{nk} \sigma_m(\omega_{kn}) \\ & \times \mathrm{Tr}\left[\mathbf{G}(\boldsymbol{r}, \boldsymbol{r}, \omega_{kn}) \cdot \mathbf{G}^*(\boldsymbol{r}, \boldsymbol{r}, \omega_{kn}) \right] \end{aligned} \tag{4}$$

where c_{nkm} is a factor that arises from use of the Wigner–Eckhart theorem, we used that $\mathbf{G}^T_{ab}(\omega) = \mathbf{G}_{ba}(\omega)$ [10] and introduced the spontaneous decay rate $\gamma_{nk} = \omega^3_{kn} |\boldsymbol{d}_{nk}|^2 / (3\pi\hbar c^3 \varepsilon_0)$. The interference term is given by:

$$\Gamma_{\mathrm{intf}} = -\sum_{n,m} \frac{2\pi \mu_0^2 \omega^2_{kn} \omega^2_{km}}{\hbar^2} \mathbf{D} : \left[\mathbf{G}(\omega_{kn}) \otimes \mathbf{G}^*(\omega_{km}) \right] \tag{5}$$

where the fourth-rank tensor $\mathbf{D}$ is defined by the transition dipoles: $\mathbf{D} = \boldsymbol{d}_{nk} \otimes \boldsymbol{d}_{mp} \otimes \boldsymbol{d}^*_{mk} \otimes \boldsymbol{d}^*_{np}$ and we denote the scalar product for dyads as: $\mathbf{A} : \mathbf{B} = A_{ijkl} B_{ijkl}$.

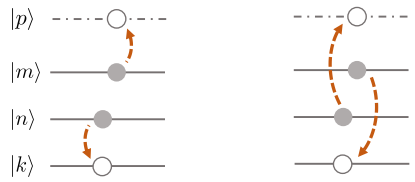

a) Direct term b) Exchange term

FIG. 1. *Level scheme for Auger decay.* An initial inner-shell vacancy $|k\rangle$ is filled by an electron from a higher energy level. Subsequently the freed energy excites another electron to the continuum state $|p\rangle$. As a consequence of their indistinguishability every direct term is paired with an exchange term, where the electrons are exchanged.

IV. REGULARISATION OF FREE-SPACE PROPAGATOR.

In free space the excitation cannot be scattered by an environment between emission and absorption and the propagator is given by the free space Green's tensor $\mathbf{G}^{(0)}$ [10]. However, as a consequence of the dipole approximation this propagator describes a *loop* propagation, which leads to a divergence. To regain a finite result we adapt a heuristic approximation that is usually used for Van-der-Waals forces between molecules whose spacing is close enough to involve significant wavefunction overlap [22]. In this approach the atom is assumed to have a finite size encoded through a spatial distribution of the polarizability $\boldsymbol{\alpha}_n(\boldsymbol{r}, \omega)$ in state $|n\rangle$, which is approximated by a Gaussian. This leads to a redefinition of the propagator for the point-like case in terms of a convolution with the Gaussian: $\mathbf{G}^{(0)}_{\mathrm{reg}}(\boldsymbol{r}_a, \boldsymbol{r}_b, \omega) = \frac{1}{\sqrt{2\pi}^3 a^3} \int \mathrm{d}V' e^{-\frac{|\boldsymbol{r}_b - \boldsymbol{r}'|^2}{2a^2}} \mathbf{G}^{(0)}(\boldsymbol{r}_a, \boldsymbol{r}', \omega)$, where a is the width of the Gaussian. For the free space Green's tensor this integral can be carried out analytically. Analogously convolving the absorption point $r_a = r_b$ with a Gaussian of the same size a we obtain in leading order of a:

$$\mathbf{G}^{(0)}_{\mathrm{reg}}(\omega) = -\frac{c^2}{24\pi^{3/2} a^3 \omega^2_{kn}} \mathbf{1} \tag{6}$$

where $\mathbf{1}$ is a 3×3 unit matrix. Combining Eq. (6) with Eqs. (4) and (5), we have developed a simple analytical tool for predicting Auger rates in free space from single–electron properties.

V. NUMERICAL EXAMPLE.

For a numerical comparison we choose a simple electronic configuration, namely the $1s2s^22p^6$ configuration that one can find in inner-shell ionised Ne^+, Na^{2+}, Mg^{3+}, etc. We use the regularised propagator for free space (6) and the Wigner–Eckhart theorem to calculate the dipole

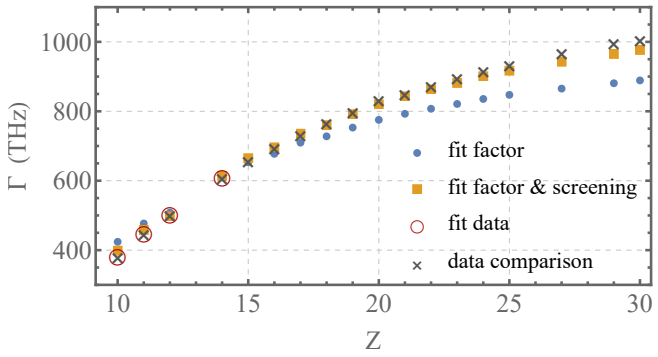

FIG. 2. *Comparison of numerical Auger rate with analytical model.* We predict the Auger rates for F-like ions with an inner vacancy via our theory by using a few known rates (red circles) to fit an overall factor for the radius model given in Eq. (8) (blue dots). This factor is determined to be $c = 1.30$ as it is also given in Tab. I in the appendix, while the screening parameter is given by the screening of the inner vacancy $S = 0.3$. The agreement with the numerical data (black crosses) gets worse with higher proton number Z. If we allow the screening parameter S to be fitted as well we reach much better agreement (yellow squares). For this fit we find a similar overall factor of $c = 1.27$ and a roughly twice as high screening of $S = 0.67$.

tensor $\mathbf{D}$ as well as the factor c_{nkm} and sum over all final states to simplify our formula for the rate to be:

$$\Gamma = 2\pi\sigma_{2p,2s}(\omega)\gamma_{2p\to 1s}\mathrm{Tr}\left[\mathbf{G}^{(0)}_{\mathrm{reg}}(\omega)\cdot\mathbf{G}^{(0)*}_{\mathrm{reg}}(\omega)\right] \qquad (7)$$

where $\sigma_{2p,2s}$ is the ionisation cross section of the L-shell. Note that the contribution to the rate given by the dipole-forbidden transition which is not included in our result is negligible in our example [23]. The predicted inverse sixth power length scaling is analogous to the asymptotic scaling in interatomic Auger decay [24] and ICD [25] where the interatomic separation appears in the latter cases in contrast to the atomic size parameter relevant here. It is reasonable to expect the Gaussian parameter a, representing the spatial width of the transition polarisability α_{nk}, to be in the order of the involved orbital sizes. These can be approximated by the Slater rules [26]: $a_{nl} = \frac{n^{*2}a_0}{Z-S}$ with a_0 being the Bohr radius and Z the number of protons, n^* the reduced quantum number and S the screening parameter. The two involved orbitals are a_{1s} and $a_{2p} = a_{2s}$. The vacancy orbital a_{1s} is much smaller and hence dominant. We use this orbital for our model with $S_{1s} = 0.3$ and $n^* = 1$. Since the choice of the profile (here Gaussian) determines the overall factor we may fit such an overall factor c to our results. The model for a is then given by:

$$a(Z) = c\frac{a_0}{Z-S} \qquad (8)$$

For the fit we use the first four data points from the numerical Auger rate data [14] and find $c = 1.30$. If we allow the screening parameter to be fit to the first four numerical values as well we find almost perfect agreement with a screening parameter of $S = 0.67$. The comparison of these models with the numerical data can be seen in Fig. 2 as well as in Tab. I in the appendix.

VI. AUGER RATE INFLUENCED BY ENVIRONMENT.

Having validated our model, the macroscopic QED approach enables us to go beyond ab initio numerics by studying the influence of different environments on the Auger rate. In equation (4) we separated the atomic properties—described for example by γ_{nk} and σ_m—from the properties of the electromagnetic field. An environment may shift the energy levels of the atom or molecule or influence the density of final electronic states. These effects are known and already studied independently of Auger decay. What we will focus on in this section is the impact of the environment onto the energy transfer between the involved electrons. As the Auger decay is thought of as an electron–electron scattering process rather than a radiating or virtual photon exchange between two electrons, this effect has been neglected so far. In the presence of an environment the Green's tensor acquires an additional contribution: $\mathbf{G}(\boldsymbol{r},\boldsymbol{r}',\omega) = \mathbf{G}^{(0)}(\boldsymbol{r},\boldsymbol{r}',\omega) + \mathbf{G}^{(1)}(\boldsymbol{r},\boldsymbol{r}',\omega)$. The additional part $\mathbf{G}^{(1)}$ is the scattering Green's tensor and describes the modification of the density of states of the field due to interfaces. As a simple example we present the influence of a dielectric half space onto the Auger rate of Ne^+. The permittivity $\varepsilon(\omega)$ of the dielectric medium is assumed to be given by the Drude–Lorentz model: $\varepsilon(\omega) = 1 - \frac{f\omega_T^2}{\omega^2-\omega_T^2+\mathrm{i}\gamma\omega}$, where f is the oscillator strength, ω_T the frequency of a material resonance and γ the damping parameter. The Drude–Lorentz model ful-

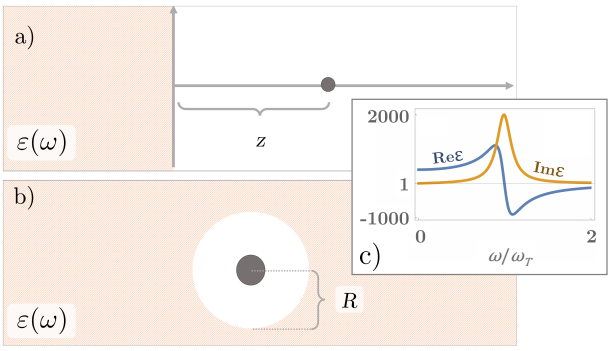

FIG. 3. *Environment effects on Auger decay* a) As a first system we introduce a dielectric half space with distance z to the Auger undergoing particle. b) As a second system we choose to embed the particle in a dielectric medium. As a simple model we describe the local field of the atom via a vacuum cavity in the medium. c) We choose a medium with a single material resonance at ω_T that can be described by the plotted permittivity $\varepsilon(\omega)$.

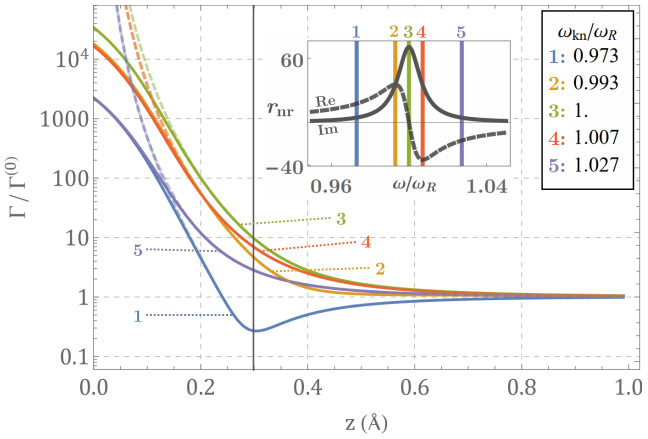

FIG. 4. The Auger rate of Ne^+ in a dielectric half space relative to the Auger rate in free space for four different medium resonances. The solid lines give the result with the regularised scattering Green's tensor $\mathbf{G}^{(1)}_{\rm reg}$ while the dashed lines give the results with $\mathbf{G}^{(1)}$. The vertical line indicates the size of the atom $a_{2p} \approx 0.3$ Å

fils the Kramers-Kronig relation and is a good model for any sharp absorption resonance, including giant dipole resonances of nuclei [27]. The scattering Green's tensor for such a system is given by:

$$\mathbf{G}^{(1)}(r_b, r_a) = \frac{\mathrm{i}}{8\pi^2}\int \frac{\mathrm{d}^2k^{\parallel}}{k^{\perp}} e^{\mathrm{i}(z_a+z_b)k^{\perp}} e^{\mathrm{i}(\boldsymbol{r}_b-\boldsymbol{r}_a)\cdot\boldsymbol{k}^{\parallel}} \times \left[r_p \boldsymbol{e}_{p+}\otimes\boldsymbol{e}_{p-} + r_s \boldsymbol{e}_{s+}\otimes\boldsymbol{e}_{s-}\right] \tag{9}$$

$$r_{s/p} = \frac{c_{s/p}\,k^{\perp} - \sqrt{\varepsilon k^2 - k^{\parallel 2}}}{c_{s/p}\,k^{\perp} + \sqrt{\varepsilon k^2 - k^{\parallel 2}}} \tag{10}$$

where $\boldsymbol{k}^{\parallel}$ denotes the part of the wave-vector parallel to the surface, $\boldsymbol{k}^{\perp}$ the perpendicular part, $\boldsymbol{e}_{\sigma\pm}$ are the polarisation unit vectors and $r_{s/p}$ are the reflection coefficients for s- and p-polarised light with $c_s = 1$ and $c_p = \varepsilon$. The geometry of the problem as well as the permittivity $\varepsilon(\omega)$ are shown in Fig. 3, where we chose $f = 400$ and $\gamma = \omega_T/5$ and placed the atom at distance z from the surface. These model parameters are inspired by the absorption resonance in sapphire [28]. In the non-retarded limit the effect of the plate is governed by the reflection coefficient $r_{\rm nr} = (\varepsilon-1)/(\varepsilon+1)$ with its evanescent-wave resonance $\varepsilon(\omega_R) \approx -1$ at $\omega_R = 14.2\,\omega_T$ for the chosen parameters. We vary the parameter ω_T, i.e. the resonance of the medium in relation to the transition frequency $\omega_{kn} \approx 850$ eV of the initial transition in Ne^+. However,treating the surface as a continuous medium leads to a diverging scattering Green's tensor in the limit of $z \to 0$. Similarly to the free space Green's tensor we can regularize the scattering Green's tensor with Gaussian convolutions of the source and absorption point $\boldsymbol{r}$:

$$\begin{aligned}\mathbf{G}^{(1)}_{\rm reg}(\boldsymbol{r},\omega) &= \frac{1}{N^2}\int_{z'>0}\mathrm{d}V' \int_{z''>0}\mathrm{d}V'' e^{\frac{|\boldsymbol{r}-\boldsymbol{r}'|^2}{2a^2}}\mathbf{G}^{(1)}(\boldsymbol{r}',\boldsymbol{r}'')e^{\frac{|\boldsymbol{r}-\boldsymbol{r}''|^2}{2a^2}} \\ &= -\frac{1}{8\pi^2}\int \frac{\mathrm{d}^2k^{\parallel}}{k^{\perp}} e^{-a^2k^2} e^{2\mathrm{i}k^{\perp}z} \\ &\quad\times\left[\frac{\mathrm{erf}\left(\frac{z}{\sqrt{2}a}+\mathrm{i}\frac{ak^{\perp}}{\sqrt{2}}\right)+1}{\mathrm{erf}\left(\frac{z}{\sqrt{2}a}\right)+1}\right]^2\end{aligned} \tag{11}$$

where $\mathrm{erf}(x)$ is the error function. Since this scattering Green's tensor only describes propagation in the half-space $z > 0$, the Gaussian convolutions are cut off at $z = 0$, hence the normalisation N for each Gaussian is given by $N = 2/\left[(2\pi)^{3/2}a^3\left(\mathrm{erf}\left[z/(\sqrt{2}a)\right]+1\right)\right]$. We can now calculate the rate by numerical integration of Eq. (11) and subsequent use of Eqs. (4) and (5). In Fig. 4 the ratio between the Auger rate in the presence of the plate Γ and the Auger rate in vacuum Γ_0 is given as a function of the atom–plate distance z. The calculation without the Gaussian regularisation gives a diverging rate in the non-retarded limit $z \to 0$, as expected, whereas the Gaussian regularisation keeps the rate finite at all positions. One observes a modification that depends on the detuning of the atomic transition from the material resonance. The strongest effect is found for zero detuning. At intermediate distances, the surface can enhance or reduce the Auger rate depending on the sign of the detuning, whereas a sign-independent enhancement is always predicted in the zero-distance limit. Note that additional effects due to electronic wave-function overlap will contribute to the Auger rate at distances smaller than the outer electron radius $a_{2p} \approx 0.3$ Å. The relative impact of the environment sensitively depends on the ratio between this radius and the radius of the vacancy which is $a_{1s}/a_{2p} \approx 7/40$ here, but can reach values of almost unity for Coster–Kronig transitions [29] with a potential enhancement of $(40/7)^6 \approx 3\times10^4$. The amplitude of the effect further depends on the height of the medium resonance, which is typically small for naturally occurring materials.

Enhancements can be provided by Bragg mirrors or x-ray waveguides [30] which can reach Q-factors of $10^2 \sim 10^3$. In general the Q-factor is given by comparing the spontaneous decay rate in the cavity γ with the rate γ_0 in free-space: $Q(3\lambda^3/4\pi^2V) = \gamma/\gamma_0 = 1 + \mathrm{Im Tr}\mathbf{G}^{(1)}(\boldsymbol{r},\boldsymbol{r})/\mathrm{Im Tr}\mathbf{G}^{(0)}(\boldsymbol{r},\boldsymbol{r})$, where V is the volume of the cavity [7]. The Purcell enhancement of the Auger rate in an x-ray resonator can be estimated by noting that the respective scattering Green's tensor can be approximated by its imaginary part $|\mathbf{G}^{(1)}| \approx |\mathrm{Im}\mathbf{G}^{(1)}|$. The free-space Green's tensor on the other hand fulfils $\mathrm{Im}\mathbf{G}^{(0)}(\boldsymbol{r},\boldsymbol{r}) = \omega/(6\pi c)\mathbf{1}$ while the free-space Auger rate $\Gamma_0 \propto |\mathbf{G}^{(0)}(\boldsymbol{r},\boldsymbol{r})|^2$ is governed by the real part of $\mathbf{G}^{(0)}$ as given by Eq. (6). With this we can relate the Auger rate in a cavity resonator Γ to the Q-factor and the free-space

Auger rate Γ_0:

$$\Gamma \approx \left(1 + s^2 b^2 Q^2 + 2sbQ\right) \Gamma_0 \tag{12}$$

$$\text{with:} \quad b = 4\sqrt{\pi}\frac{\omega^3 a^3}{c^3} \ll 1 \quad \text{and} \quad s = \frac{3\lambda^3}{4\pi^2 V} \tag{13}$$

To achieve a significant enhancement of the Auger decay in a cavity the Q-factor must be much larger than the factor b. In the example of neon $b_{\mathrm{Ne}} = 0.004$, hence for $sQ \geq 200$ the Auger decay would be enhanced significantly. Auger decay can similarly be enhanced or suppressed for other Auger atoms or quantum dots. The cavity resonance can then be much lower (f.e. in Auger-undergoing doubly excited helium $\omega_{kn} \approx 40$ eV [31]).

As a second example for the influence by environment we calculate the Auger rate for a particle embedded in a bulk medium described by the same $\varepsilon(\omega)$-model. The system is schematically given in Fig. 3b). We use the real-cavity model to account for local-field corrections [32], which entails enclosing the atom in a small spherical free-space cavity of radius R. Using the respective Green's tensor [33], we can calculate the Auger rate, the calculation is sketched in the appendix. Applying the non-retarded limit $\omega R/c \ll 1$ and $\omega a/c \ll 1$ we may give an expression for the medium assisted Auger rate where one can estimate the influence of a given permittivity ε:

$$\Gamma = \Gamma^{(0)}\left(1 - \frac{24\sqrt{\pi}a^3}{R^3}\mathrm{Re}\left[\frac{1-\varepsilon}{1+2\varepsilon}\right] + \frac{144\pi a^6}{R^6}\left|\frac{1-\varepsilon}{1+2\varepsilon}\right|^2\right) \tag{14}$$

The exact relative Auger rate (B5) as a function of the cavity radius is given in the appendix and is plotted in Fig. 5 for Ne^+, where we used the full expression (B5). The rate is given in a range of $a_{2p} < R < 5a_{2p}$, assuming that $a_{2p} \approx 0.6a_0$ gives a rough estimate for the size of the atom. Depending on the medium resonance one can achieve enhancement and suppression of the Auger rate up to several orders due to local field effects (i. e. the difference between the macroscopic field in the medium and the microscopic field experienced by the Auger atom). In contrast to the surface-induced effect, the medium-induced modification depends on the detuning with respect to the Mie-resonance $\omega'_R = 16.6\,\omega_T$, as seen from Eq. (14).

VII. CONCLUSION.

In this work we have extended the domain of quantum optics to Auger decay. We derived an approximate analytical expression for the Auger rate in free space and found very good agreement to numerical data. We presented two simple examples of how the Auger decay rate might be influenced by a nearby medium. In case of a dielectric half-space we introduced a regularisation for small distances between plate and atom. By choosing generic single x-ray-resonance material we could obtain an influence of several orders for both cases. Our free-space rate formula can serve to approximate the expected Auger rate in experiments, and by studying different isoelectronic sequences we may determine a precise model for the radius-like Gaussian parameter. Now that the Auger process can be studied by quantum optical methods and in different environments one can study systems where ICD and Auger occur together, competing or initiating each other [31, 34]. One could modify the environment to enhance one process while suppressing the other or to optimize cascade-like relaxation chains. Furthermore the Gaussian regularisation that is used in this work to regularize the Green's tensor can serve for other second order energy transfer rates (e.g. ICD or FRET) to obtain finite rates in the limit of very small distances. Such rates are currently unknown for the dissipative processes relevant to current experiments involving heavy-ion scattering off 2d materials [35, 36].

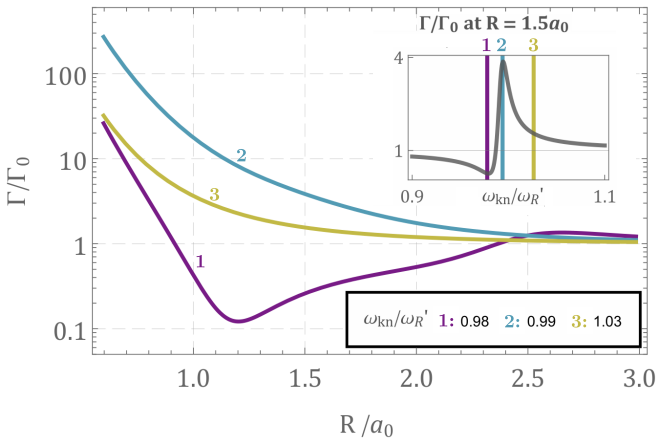

FIG. 5. The Auger rate Γ of Ne^+ in a medium relative to the free space rate Γ_0. The system is described approximately by the real cavity model and the rate is given as a function of the radius R of this cavity. The resonance of the medium surrounding the atom is varied around the transition energy ω_{kn} of the Auger decay.

ACKNOWLEDGMENTS

The authors thank A. Burkert, L. S. Cederbaum, K. Gokhberg, T. Janka, M. Kowalewski, P. Schmelcher, N. Sisourat for discussions. This work was supported by the German Research Foundation (DFG, Grants No. BU 1803/3-1 and No. GRK 2079/1).

Appendix A: Comparison of the model to the numerical data

We compare our analytic approximate formula for the Auger decay in free space (7), see main text, to available numerical data for two different models for the Gaussian

Z	fit factor in THz (%)	fit screening in THz (%)	numerical Γ [14] in THz
10	424 (110)	399 (104)	385
11	477 (106)	458 (102)	450
12	508 (100)	497 (98)	506
14	610 (99)	614 (100)	613
15	653 (99)	665 (101)	660
16	677 (97)	696 (100)	699
17	710 (96)	735 (100)	736
18	728 (95)	760 (99)	769
19	753 (94)	792 (99)	802
20	775 (93)	820 (98)	837
21	793 (93)	843 (99)	853
22	807 (92)	863 (98)	877
23	821 (91)	882 (98)	900
24	836 (91)	901 (98)	919
25	847 (90)	917 (98)	938
27	865 (89)	943 (97)	972
29	881 (88)	965 (97)	1000
30	889 (88)	977 (97)	1010

TABLE I. Comparison of the Auger rate calculated by the analytic formula (7) with two different Gaussian parameter models for a and the numerical calculated rates found in [14]. In the braces the calculated rate is given in percentage relative to the numerical value.

parameter a. The respective unknown parameters are found by fitting the respective model to the first four numerical data of the isoelectronic sequence of Ne^+. In the first case we use the 1s-radius given by Slater [26] and fit an overall factor $c_{\rm fit} = 1.3$ in front of it, while in the second case we also let the screening factor be determined by the fit. In this second case we find $S_{\rm fit} = 0.67$ and a similar overall factor of $c'_{\rm fit} = 1.27$. The comparison is shown in Table I as well as in Fig. 2 in the main text.

Appendix B: Derivation of Auger rate in a medium.

As an example for an macroscopic environment that may enhance or suppress the Auger rate we embed the respective atom in a medium. This medium can be macroscopically described in different ways, one of which is the real cavity model which we choose to present here. In this model the atom is enclosed in a spherical free-space cavity of radius R. The scattering Green's tensor $\mathbf{G}^{(1)}(\boldsymbol{r}_2, \boldsymbol{r}_1, \omega) = \mathbf{G}^{(1)}_{12}(k_0 = \omega/c)$ can be easily calculated by solving the boundary conditions for the Helmholtz equation with the general ansatz:

$$\begin{aligned}\mathbf{G}^{(1)}_{12} = \frac{\mathrm{i}}{4\pi k_0}\sum_{p\in\{e,o\}}\sum_{n=1}^{\infty}\sum_{m=0}^{n}(2-\delta_{m0})\frac{(2n+1)(n-m)!}{n(n+1)(n+m)!}\\ \times\Big\{\big[c_n^v \boldsymbol{V}_{pmn}(k_0,\boldsymbol{r}_2) + c_n^w \boldsymbol{W}_{pmn}(k_0,\boldsymbol{r}_2)\big]\\ \otimes \boldsymbol{V}_{pmn}(k_0,\boldsymbol{r}_1)\\ \times +\big[d_n^v \boldsymbol{V}_{pmn}(k_0,\boldsymbol{r}_2) + d_n^w \boldsymbol{W}_{pmn}(k_0,\boldsymbol{r}_2)\big]\\ \otimes \boldsymbol{W}_{pmn}p(k_0,\boldsymbol{r}_1)\Big\}\end{aligned} \tag{B1}$$

where $\boldsymbol{V}$ and $\boldsymbol{W}$ are base functions for the electromagnetic wave, describing the propagation of right and left circularly polarized light, respectively and are given by a symmetric and antisymmetric combination of the spherical vector magnetic and electric harmonics, $\boldsymbol{M}^{e}_{o}{}_{mn}(k,\boldsymbol{r})$ and $\boldsymbol{N}^{e}_{o}{}_{mn}(k,\boldsymbol{r})$:

$$\begin{aligned}\boldsymbol{V}^{e}_{o}{}_{mn}(k,\boldsymbol{r}) &= \frac{\boldsymbol{M}^{e}_{o}{}_{mn}(k,\boldsymbol{r}) + \boldsymbol{N}^{e}_{o}{}_{mn}(k,\boldsymbol{r})}{\sqrt{2}} \\ &= \frac{1}{\sqrt{2}}\Bigg[\mp\frac{m}{\sin(\theta)}P_{nm}(\cos(\theta))\begin{matrix}\sin\\\cos\end{matrix}(m\phi)\\ &\quad\times\left(j_n(kr)\boldsymbol{e}_\theta + \frac{1}{kr}\frac{\partial}{\partial r}[rj_n(kr)]\boldsymbol{e}_\phi\right)\\ &\quad+\frac{\partial P_{nm}(\cos(\theta))}{\partial\theta}\begin{matrix}\cos\\\sin\end{matrix}(m\phi)\\ &\quad\times\left(\frac{1}{kr}\frac{\partial}{\partial r}[rj_n(kr)]\boldsymbol{e}_\theta - j_n(kr)\boldsymbol{e}_\phi\right)\\ &\quad+n(n+1)P_{nm}(\cos(\theta))\begin{matrix}\cos\\\sin\end{matrix}(m\phi)\\ &\quad\times\frac{j_n(kr)}{kr}\boldsymbol{e}_r\Bigg]\end{aligned} \tag{B2}$$

$$\begin{aligned}\boldsymbol{W}^{e}_{o}{}_{mn}(k,\boldsymbol{r}) &= \frac{\boldsymbol{M}^{e}_{o}{}_{mn}(k,\boldsymbol{r}) - \boldsymbol{N}^{e}_{o}{}_{mn}(k,\boldsymbol{r})}{\sqrt{2}} \\ &= \frac{1}{\sqrt{2}}\Bigg[\mp\frac{m}{\sin(\theta)}P_{nm}(\cos(\theta))\begin{matrix}\sin\\\cos\end{matrix}(m\phi)\\ &\quad\times\left(j_n(kr)\boldsymbol{e}_\theta - \frac{1}{kr}\frac{\partial}{\partial r}[rj_n(kr)]\boldsymbol{e}_\phi\right)\\ &\quad+\frac{\partial P_{nm}(\cos(\theta))}{\partial\theta}\begin{matrix}\cos\\\sin\end{matrix}(m\phi)\\ &\quad\times\left(-\frac{1}{kr}\frac{\partial}{\partial r}[rj_n(kr)]\boldsymbol{e}_\theta - j_n(kr)\boldsymbol{e}_\phi\right)\\ &\quad-n(n+1)P_{nm}(\cos(\theta))\begin{matrix}\cos\\\sin\end{matrix}(m\phi)\\ &\quad\times\frac{j_n(kr)}{kr}\boldsymbol{e}_r\Bigg]\end{aligned} \tag{B3}$$

The reflection coefficients can then be found by solving the boundary conditions at $r = R$. We are interested in the propagation form $\boldsymbol{r}_1 = 0$ to $\boldsymbol{r}_2 = 0$, in this case only $n = 1$ gives non-vanishing contributions to $\mathbf{G}^{(1)}$:

$$\begin{aligned}\mathbf{G}^{(1)}(0,0,k_0) &= \frac{\mathrm{i}}{12\pi k_0}(c_1^v - c_1^w - d_1^v + d_1^w)\mathbf{1} \\ &= -\mathrm{i}\frac{k_0}{6\pi D}\big(n^2 h_1 h_1' - n^2 k_0 R h_2 h_1' \\ &\quad + n^2 k_0 R h_0 h_1' - n k_0 R h_1 h_0' \\ &\quad + n k_0 R h_1 h_2' - h_1 h_1'\big) \qquad \text{(B4)} \\ D &= n^2 k_0 R(j_0 - j_2)h_1' + j_1((n^2-1)h_1' \\ &\quad - n k_0 R h_0' + n k_0 R h_2') \qquad \text{(B5)}\end{aligned}$$

where $n = \sqrt{\varepsilon\mu}$ is the refractive index and we used the shorthand notation: $j_m = j_m(k_0 R)$, $j_m' = j_m(n k_0 R)$ are the spherical Bessel functions and $h_m = h_m^{(1)}(k_0 R)$, $h_m' = h_m^{(1)}(n k_0 R)$ are the spherical Hankel functions of first kind. For $k_0 R \ll 1$ we find in leading order of $k_0 R$:

$$\mathbf{G}^{(1)}(k_0) \approx \frac{1}{2\pi k_0^2 R^3}\frac{\varepsilon - 1}{2\varepsilon + 1}\mathbf{1} \qquad \text{(B6)}$$

The rate is given by:

$$\begin{aligned}\Gamma &= 2\pi\gamma_{nk}\sigma_m(\omega_{kn})\mathrm{Tr}\left[\mathbf{G}(\omega_{kn})\cdot\mathbf{G}^{T*}(\omega_{kn})\right] \qquad \text{(B7)} \\ &= 2\pi\gamma_{nk}\sigma_m(\omega_{kn})\mathrm{Tr}\Big[\mathbf{G}^{(0)}(\omega_{kn})\cdot\mathbf{G}^{(0)*}(\omega_{kn}) \\ &\quad + \mathbf{G}^{(1)}(\omega_{kn})\cdot\mathbf{G}^{(1)*}(\omega_{kn}) \\ &\quad + 2\mathrm{Re}(\mathbf{G}^{(0)}(\omega_{kn})\cdot\mathbf{G}^{(1)*}(\omega_{kn}))\Big]\end{aligned}$$

In the limit of $k_0 R = \omega_{kn} R/c \ll 1$ we therefore find:

$$\begin{aligned}\Gamma \approx \Gamma^{(0)}\Bigg(1 &- \frac{24\sqrt{\pi}a^3}{R^3}\mathrm{Re}\left[\frac{1-\varepsilon}{1+2\varepsilon}\right] \\ &+ \frac{144\pi a^6}{R^6}\left|\frac{1-\varepsilon}{1+2\varepsilon}\right|^2\Bigg) \qquad \text{(B8)}\end{aligned}$$

with:

$$\Gamma^{(0)} = 2\pi\gamma_{nk}\sigma_m(\omega_{kn})\mathrm{Tr}\left[\mathbf{G}^{(0)}(\omega_{kn})\cdot\mathbf{G}^{(0)*}(\omega_{kn})\right] \qquad \text{(B9)}$$

and $\mathbf{G}^{(0)}(\omega_{kn})$ is given in first order by Eq. (6).

[1] T. Förster, Ann. Phys. **437**, 55 (1948).
[2] A. Salam, Atoms **6**, 56 (2018).
[3] G. A. Jones and D. S. Bradshaw, Front. Phys. **7**, 100 (2019).
[4] L. S. Cederbaum, J. Zobeley, and F. Tarantelli, Phys. Rev. Lett. **79**, 4778 (1997).
[5] K. Gokhberg, P. Kolorenč, A. I. Kuleff, and L. S. Cederbaum, Nature **505**, 661 (2014).
[6] B. Boudaïffa, P. Cloutier, D. Hunting, M. A. Huels, and L. Sanche, Science **287**, 1658 (2000).
[7] E. M. Purcell, in *Proceedings of the American Physical Society*, Vol. 69 (American Physical Society, 1946) p. 674.
[8] K. Drexhage, J. Lumin. **1-2**, 693 (1970).
[9] J. L. Hemmerich, R. Bennett, and S. Y. Buhmann, Nat. Commun. **9**, 2934 (2018).
[10] S. Y. Buhmann, *Dispersion forces I: Macroscopic quantum electrodynamics and ground-state Casimir, Casimir–Polder and van der Waals Forces*, Vol. 247 (Springer, 2013).
[11] P. Auger, Comptes rendus l'Académie des Sci. **177**, 169 (1923).
[12] L. Meitner, Z. Phys. **11**, 35 (1922).
[13] K. Bennett, M. Kowalewski, and S. Mukamel, Faraday Discuss. **177**, 405 (2015).
[14] P. Palmeri, P. Quinet, C. Mendoza, M. A. Bautista, J. Garcia, and T. R. Kallman, Astrophys. J. Suppl. Ser. **177**, 408 (2008).
[15] A. Ku, V. J. Facca, Z. Cai, and R. M. Reilly, EJNMMI Radiopharm. Chem. **4**, 27 (2019).
[16] K. G. Hofer, in *Acta Oncol.*, Vol. 39 (2000) pp. 651–657.
[17] D. M. Riffe, G. K. Wertheim, and P. H. Citrin, Phys. Rev. Lett. **63**, 1976 (1989).
[18] C. D. Wagner and A. Joshi, J. Electron Spectros. Relat. Phenomena **47**, 283 (1988).
[19] D. Chattarji, in *The Theory of Auger Transitions* (Academic Press, 1976) pp. 13–29.
[20] C. Møller, Ann. Phys. **406**, 531 (1932).
[21] R. C. Hilborn, Am. J. Phys. **50**, 982 (1982).
[22] J. Mahanty and B. W. Ninham, *Dispersion forces*, Colloid science (Academic Press, 1976).
[23] P. Kolorenč and V. Averbukh, J. Chem. Phys. **135**, 134314 (2011).
[24] J. Matthew and Y. Komninos, Surface Science **53**, 716 (1975).
[25] R. Santra and L. S. Cederbaum, Physics Reports **368**, 1 (2002).
[26] J. C. Slater, Phys. Rev. **36**, 57 (1930).
[27] Y.-J. Chen, S. Pabst, A. Karamatskou, and R. Santra, Phys. Rev. A **91**, 032503 (2015).
[28] S. Scheel and S. Y. Buhmann, Phys. Rev. A **80**, 042902 (2009).
[29] L. Jenkins and M. Chung, Surface Science **24**, 125 (1971).
[30] T. Salditt, S. Hoffmann, M. Vassholz, J. Haber, M. Osterhoff, and J. Hilhorst, Phys. Rev. Lett. **115**, 203902 (2015).
[31] G. Jabbari, K. Gokhberg, and L. S. Cederbaum, Chemical Physics Letters **754**, 137571 (2020).

[32] J. Fiedler, P. Thiyam, A. Kurumbail, F. A. Burger, M. Walter, C. Persson, I. Brevik, D. F. Parsons, M. Boström, and S. Y. Buhmann, J. Phys. Chem. A **121**, 9742 (2017).
[33] L. W. Li, P. S. Kooi, M. S. Leong, and T. S. Yeo, IEEE Trans. Microw. Theory Tech. **42**, 2302 (1994).
[34] S. D. Stoychev, A. I. Kuleff, F. Tarantelli, and L. S. Cederbaum, J. Chem. Phys. **129**, 074307 (2008).
[35] R. A. Wilhelm, E. Gruber, J. Schwestka, R. Kozubek, T. I. Madeira, J. P. Marques, J. Kobus, A. V. Krasheninnikov, M. Schleberger, and F. Aumayr, Phys. Rev. Lett. **119**, 103401 (2017).
[36] R. A. Wilhelm and P. L. Grande, Commun. Phys. **2**, 89 (2019).